Rapid vs. Delayed Infrared Responses after Ischemia Reveal Recruitment of Different Vascular Beds

by *K. Chang, *M. Antalek, *M. Seidel, *T. Darlington, **A. Ikeda, **T.C. Anaebere, *S. Yoon, ***C. Seamon, ***G.J. Kato, **H. Ackerman, and *A.M. Gorbach

*Infrared Imaging and Thermometry Unit, National Institute of Biomedical Imaging and Bioengineering, National Institutes of Health, 9000 Rockville Pike, Building 13, Bethesda, MD 20892, USA; gorbacha@mail.nih.gov
**The Laboratory of Malaria and Vector Research, National Institute of Allergy and Infectious Diseases, National Institutes of Health, 12735 Twinbrook Pkwy, Rockville, MD, 20852, USA
***The Hematology Branch, National Heart, Lung, and Blood Institute, National Institutes of Health, 31 Center St, Bethesda, MD 20892
****Division of Hematology/Oncology, Vascular Medicine Institute, University of Pittsburgh Medical Center, 200 Lothrop Street, Pittsburgh, PA 15261, USA

Abstract

To identify vascular dysfunction in sickle cell disease patients, we compared transient changes in forearm temperature during arterial occlusion, reperfusion, and recovery in Healthy, Sickle Cell Steady State, Sickle Cell Pain Crisis, and Recovered from Pain Crisis subject groups. Combining this test with continuous infrared imaging followed by image processing with the *k-means* algorithm revealed reactive vascular sites in the skin where rapid and delayed temperature amplification were statistically different between subject groups. Observed temporal and spatial diversity of blood flow-derived forearm temperature allow consideration of thermographically guided placement of skin sensors for more sensitive monitoring of skin hemodynamics.

1. Introduction

Sickle Cell Disease (SCD) is a hereditary disorder caused by a point mutation in the β-globin gene, which leads to the formation of sickle hemoglobin (hemoglobin S). One unique characteristic of SCD among hemolytic anemias is episodes of painful vaso-occlusive crises that have unpredictable onset and duration [1]. Although there is no single explanation for these episodes, there are several contributing mechanisms that may act synergistically. Sickled cells have an increased adherence to endothelial cells, which may slow blood flow [2]. Sickled cells also alter endothelium-dependent events, with mechanisms including diminished vasodilation in response to shear stress and diminished response to nitric oxide due to cell-free ferrous hemoglobin in the plasma [3, 4]. As small and large vessels become occluded, further adherence of sickled cells to endothelial cells and vasoconstriction may occur [5]. Despite the identification of these mechanisms, little is known about the cumulative effect of the disease on the skin's vascular architecture, known as the angiosome [6]. The objective of this work was to characterize skin temperature in SCD patients as well as quantitatively distinguish changes in blood flow in the Healthy Volunteer (HV), Sickle Cell Steady State (ST), Sickle Cell Pain Crisis (PC), and Recovered from Pain Crisis (RC) groups.

Although techniques exist to measure micro- and macro-circulation in skin (capillaroscopy, laser Doppler flowmetry, laser speckle contrast, and photoplethysmography) and within skeletal muscle (Doppler ultrasound), infrared (IR) imaging provides the advantage of being a modality capable of accessing cutaneous and subcutaneous vessels simultaneously. This is because IR imaging captures the conduction and convection of heat to the surface of the skin. Other studies have used high resolution IR imaging to assess blood flow in rat kidneys and human brains [7, 8]. A study by Gorbach et al. showed that skin temperature correlated significantly with forearm blood flow [9]. To assess blood flow in the different subject groups, the post-occlusive reactive hyperemia (PORH) test, a standard test of circulatory function, was combined with IR imaging of the volar aspect of the forearm. The PORH test also created conditions favoring increased intracellular hemoglobin S polymerization in the SCD patients through hypoxemia, stagnant flow, and acidosis [10]. IR measurements were validated through comparison with blood flux measurements using laser Doppler flowmetry (LDF) probes. We hypothesize that temporal and spatial heterogeneity in skin hyperemic responses to ischemia, measured by IR imaging, can be utilized to delineate differences in peripheral blood flow among the subject groups.

2. Methods
2.1 Study Population

38 HV, 29 ST, 20 PC, and 18 RC subjects were enrolled. Studies were performed on RC subjects again more than three weeks after the resolution of pain crisis symptoms. All subjects were on an approved protocol 12-H-0101 and provided written informed consent. See http://www.clinicaltrials.gov/ct2/show/NCT01568710 for enrollment criteria. Subjects were

between 18 and 70 years of age. IR imaging studies from 4 HV, 2 ST, 4 PC, and 3 RC subjects were excluded due to excessive patient movement.

2.2 PORH Test

Upon arrival at the NIH Clinical Center between 11 AM and 12 PM, subjects were placed in a temperature-controlled room (21.1 ± 0.9°C). Temperature fluctuations in the room were recorded continuously with a data logger (Datalogger 42270, Extech Instruments, USA). The subjects were seated in a hospital bed inclined at a 45° angle, with either the left or right hand secured to a padded armrest at heart level with the volar aspect of the forearm facing upward. All subjects were instructed to remain as still as possible during imaging, and a Velcro strap was used to minimize involuntary movements. Prior to the post-occlusive reactive hyperemia test, all subjects were given a 20 min period of acclimatization to the room. During the test, full occlusion of the left arm was achieved by automated inflation of an upper arm blood pressure cuff (moorVMS-PRES, Moor Instruments, Inc., USA) to at least 60 mmHg above systolic pressure for 5 min followed by cuff deflation.

2.3 IR Imaging

A cooled IR camera (Santa Barbara FocalPlane Array, Lockheed Martin, USA) was positioned 42 cm above the volar aspect of the subject's forearm (figure 1) and was remotely focused on three triangular thermo-reflective pieces of tape placed on the skin as fiducial markers. In total, 5820 IR images (640×512 pixels per image) were collected, with each 50 min PORH test consisting of 30 min of baseline, 5 min of occlusion, and 15 min of post-occlusion. IR images were acquired in the 3.0–5.0 μm wavelength range at 1.94 Hz (WinIR software, Lockheed Martin, USA). The camera was able to resolve two adjacent pixels that differed by 0.015 °C. Temperature calibration was performed prior to imaging as previously described [9]. IR images were displayed in real time allowing immediate observation of gross changes in arm perfusion. The IR images were then saved as an image cube for subsequent offline analysis.

2.4 LDF

LDF (moorVMS-LDF, Moor Instruments, Inc., USA) was performed on all subjects to measure blood flux concurrently with IR imaging. Three LDF probes were attached to the subject's skin using double-sided sticky O-rings in a line along the medial side of the forearm near the antecubital space, close to the skin area imaged by IR (figure 1). Skin blood flux values were collected at 40 Hz for each probe using a 785 nm red laser light source during the 50 min PORH test. The flux values were then saved for subsequent offline analysis.
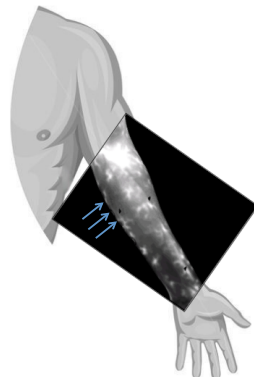

Fig. 1. Representative IR Image overlying left volar aspect of the left forearm. Bright areas indicate regions with higher skin temperature while dark areas indicate regions with lower skin temperature. The fiducial markers (three pieces of thermo-reflective tape) appear as three dark triangles on the IR image. The three blue arrows indicate the positioning of the three LDF probes.

2.5 IR Image Processing

All processing of IR images was performed in MATLAB (R2012b, MathWorks, USA). To reduce motion artifacts, rigid-body image registration was performed by maximizing the cross correlation with a chosen reference frame. The IR image intensity units were converted to temperature units (°C) based on a previously stored calibration file.

To define the whole region of interest (W_{ROI}) for each subject, the volar aspect of the forearm between the wrist and the antecubital space was manually circumscribed on IR images off-line, and time-temperature profiles were calculated for each pixel. To investigate the vascular responses of different territories, the integral of the absolute value of the 1st derivative within 0-120 s of reperfusion was calculated for each time-temperature profile within the W_{ROI}, generating an image where each pixel represented the integral value. Following spatial smoothing (4x4 pixel moving average), *k-means* (a method to partition pixels into clusters based on the nearest mean [11]) was implemented in the image to classify pixels as either part of the reactive region of interest (R_{ROI}, pixels with high integral values) or part of the non-reactive region of interest (NR_{ROI}, pixels with low integral values) (figure 2, Step I). Next, time-temperature profiles were extracted for each pixel again, but now within the R_{ROI}. The variance within 0-120 s of reperfusion was calculated for each time-temperature profile, generating an image where each pixel represented the variance value. Following spatial smoothing (4x4 pixel moving average), *k-means* clustering was implemented in the resulting image to classify pixels as either part of the early reactive region of interest (ER_{ROI}, pixels with high variance) or part of the late reactive region of interest (LR_{ROI}, pixels with low variance) (figure 2, Step II).
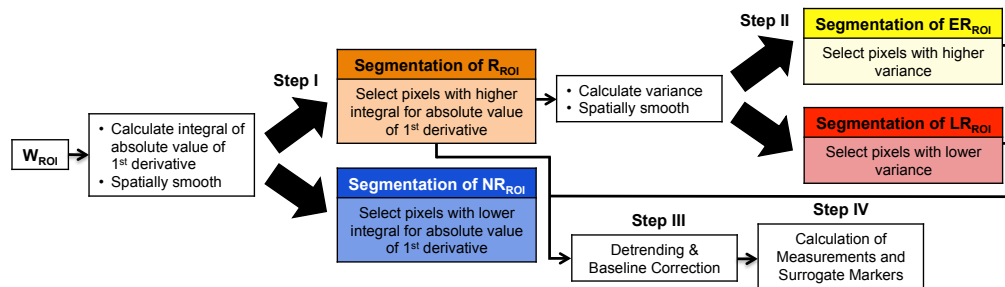
*Fig. 2. Flow diagram of image processing for each subject: classification (Steps I and II), detrending and baseline correction (Step III), and temporal marker calculation (Step IV).*
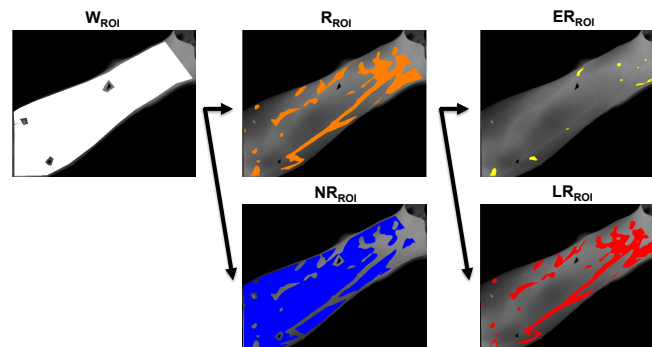
Fig. 3. Classification results of R_{ROI}, NR_{ROI}, ER_{ROI}, and LR_{ROI} (Steps I and II, representative subject).

Detrending and baseline correction procedures (figure 2, Step III) were implemented to eliminate a cooling trend observed in the IR-derived temperature data. Time-temperature profiles were extracted from the R_{ROI}, ER_{ROI}, LR_{ROI}, and NR_{ROI} over the 50 min duration of imaging and were spatially averaged within each ROI. The time-temeprature profiles from the R_{ROI}, ER_{ROI}, and LR_{ROI} were detrended by subtracting the time-temperature profile of the NR_{ROI}, to delineate the temperature response of the reactive regions relative to the nonreactive regions. To account for different cooling trends in the R_{ROI}, ER_{ROI}, and LR_{ROI} compared to the NR_{ROI}, baseline correction was applied to the detrended time-temperature profiles of the R_{ROI}, ER_{ROI}, and LR_{ROI}. Baseline correction consisted of first creating an approximation of the trend by taking a moving average (232 s time window) of the first 26 min of the baseline period and the last 25 s of the study, and by linearly interpolating the time period in between. Each ROI's trend approximation was then subtracted from the corresponding detrended time-temperature profile.

To quantify differences in the dynamics of the PORH-derived temperature profiles, measurements for the R_{ROI}, ER_{ROI}, and LR_{ROI} were calculated from the detrended, baseline-corrected time-temperature profiles for each subject (Step IV, table 1). Finally, surrogate markers (table 2) were calculated using these measurements.
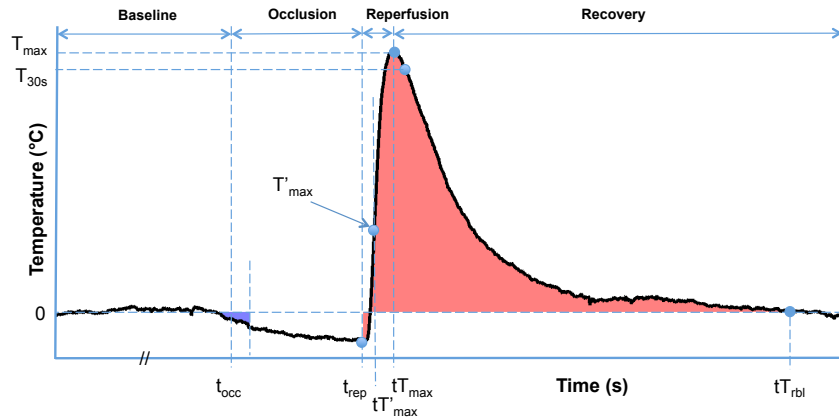
Fig. 4. *Detrended, baseline corrected time-temperature profile (representative subject) with segments of PORH test and measurements labeled.*

Table 1. *Definition of measurements derived from the detrended, baseline-corrected time-temperature profiles. Note: m°C represents millidegree Celsius.*

Measurements	Definition
t_{occ}	Time point corresponding to the start of occlusion (s)
t_{rep}	Time point corresponding to start of reperfusion (s)
T'_{max}	Maximum temperature derivative during reperfusion (m°C / s)
tT'_{max}	Time point corresponding to T'_{max} (s)
T_{max}	Temperature corresponding to the peak of post occlusive response (°C)
tT_{max}	Time point corresponding to T_{max} (s)
T_{30s}	Temperature corresponding to 30 s after tT_{max} (°C)
tT_{rbl}	Time point at which temperature returns to baseline after tT_{max} (s)

Table 2. *Surrogate markers calculated from derived measurements. All temporal markers were calculated after detrending and baseline correction except for Baseline Temperature, which is the pre-processed temperature. First 60 s Occlusion and Reperfusion and Recovery shaded in blue and red, respectively, in figure 4.*

| Surrogate Marker	Definition
R_{ROI} (% of W_{ROI})	R_{ROI} / W_{ROI} * 100
ER_{ROI} (% of W_{ROI})	ER_{ROI} / W_{ROI} * 100
LR_{ROI} (% of W_{ROI})	LR_{ROI} / W_{ROI} * 100
Baseline Temperature (°C)	Mean temperature between (t_{occ} - 300 s) and t_{occ}
First 60 s Occlusion (°C * s)	$\int T(t)\, dt$ between t_{occ} and (t_{occ} + 60 s)
T_{max} (°C)	T_{max}
T_{min} (°C)	T_{min}
$\Delta t_{tTmax - trep}$ (s)	tT_{max} - t_{rep}
$\Delta t_{tT'max - trep}$ (s)	tT'_{max} - t_{rep}
$\Delta t_{tTmax - tT'max}$ (s)	tT_{max} - tT'_{max}
Slope (m°C / s)	Mean temperature derivative between t_{rep} and tT'_{max}
Reperfusion and Recovery (°C * s)	$\int T(t)\, dt$ between t_{rep} and tT_{rbl}
First 30 s of Recovery	$(T_{max} - T_{30s}) / T_{max}$
Recovery Time (s)	tT_{rbl} - tT_{max}

2.6 Statistical Analysis

Mann-Whitney tests were used to compare ST to HV subject groups, and PC to ST subject groups. Paired Wilcoxon signed rank tests were used to compare RC to PC subject groups for the 13 patients who underwent imaging during both pain-crisis and recovery.

3. Results
3.1 Reactive Regions Show Amplified Response to Occlusion and Ischemia

For HV subjects (n=34), 15.2% of the W_{ROI} pixels were classified as R_{ROI} (figure 5a). R_{ROI} showed a significant amplification in signal-to-baseline during both occlusion and reperfusion compared to the W_{ROI} (figure 5b).
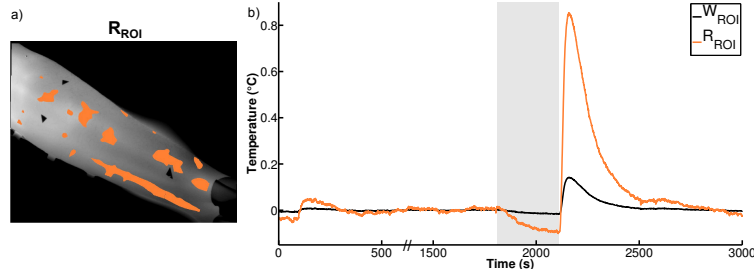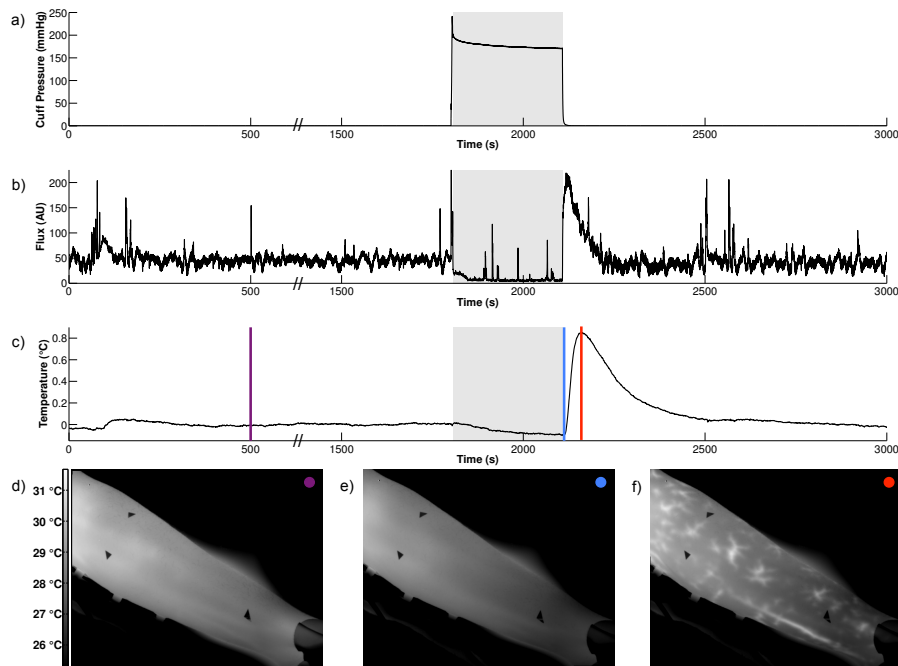

Fig. 5. *(a) Computed R_{ROI} (clusters of orange pixels) overlying the raw IR image of a representative HV subject's forearm. (b) Time-temperature profiles of the W_{ROI} (black) and R_{ROI} (orange) for the same subject. Both profiles are detrended and baseline-corrected. The occlusion segment is highlighted in gray.*

The median T_{max} for W_{ROI} was 0.033 °C while the median T_{max} for the R_{ROI} was 0.25 °C ($p < 0.01$) for healthy volunteers. The median T_{min} for W_{ROI} was -0.03 °C while the median T_{min} for the R_{ROI} was -0.31 °C ($p < 0.01$) for the same group. Assessing only the most reactive vasculature emphasized the differences among the subject groups.

## 3.2 IR Imaging Reflects Changes in Forearm Blood Flow during PORH Test

The PORH test showed change of IR-derived temperature on all measurements (n=92). IR revealed both temporal (figure 6c) and spatial (figure 6d-f) changes for each subject. A general similarity between the LDF time-flux profile (figure 6b) and time-temperature profile of the R_{ROI} (figure 6c) was noted for the occlusion, reperfusion, and recovery segments of the PORH test. It should be noted, compared with time-flux profile, the time-temperature profile displayed a delayed response during occlusion and prolonged responses during reperfusion and recovery. For the HV subject group, the time between reperfusion start and the peak LDF response was 11 s (median), while the time between reperfusion start and the peak temperature response ($\Delta t_{tTmax - trep}$) within the R_{ROI} was 94 s (median, $p < .001$). The group median Spearman's correlation coefficient between time-flux and time-temperature profiles for HV subjects was 0.19 ($p < 0.01$).

3.3 IR Imaging Revealed Spatial Blood-Flow-Derived Temperature Heterogeneity

In general, ER$_{ROI}$ consisted of small isolated regions, while LR$_{ROI}$ were the areas surrounding ER$_{ROI}$ as well as large venous structures (figure 3). The percentage of R$_{ROI}$, ER$_{ROI}$, and LR$_{ROI}$ pixels within the W$_{ROI}$ were calculated for all subject groups. The PC group had a higher percent of pixels than the RC subject group for R$_{ROI}$ ($p < 0.01$, figure 7), ER$_{ROI}$ ($p < 0.01$), and LR$_{ROI}$ ($p < 0.05$).
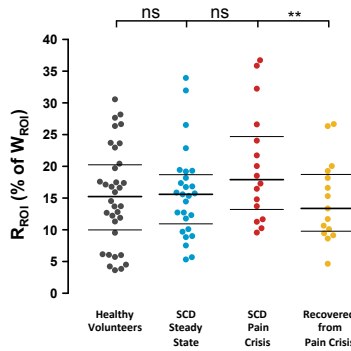
Fig 7. Percent of pixels for R$_{ROI}$ of HV, ST, PC, and RC groups. Significance levels indicated by **p < 0.01 and ns (not significant).

Table 3. Calculated spatial surrogate markers for HV, ST, PC, and RC groups. Data presented as median (interquartile range). p < 0.05 for RC compared to PC (‡). Statistically significant comparisons between a subject group and the subject group immediately to its left are highlighted.

Surrogate Marker	Healthy Volunteer (n=34)	Sickle Cell Steady State (n=27)	Sickle Cell Pain Crisis (n=16)	Recovered from Pain Crisis (n=15)
R$_{ROI}$ (% of W$_{ROI}$)	15.2 (9.5, 20.4)	15.6 (10.5, 18.9)	17.9 (12.7, 25.3)	13.4 (9.6, 19)‡
ER$_{ROI}$ (% of W$_{ROI}$)	2 (1.2, 3.1)	2.3 (0.7, 3.5)	1.9 (1.5, 3)	1.1 (0.8, 2.1)‡
LR$_{ROI}$ (% of W$_{ROI}$)	11.9 (7.8, 16.2)	12.6 (9, 16.1)	15.2 (10.8, 23.5)	12.3 (8.3, 17.9)‡

3.4 IR Imaging Revealed Temporal Blood-Flow-Derived Temperature Heterogeneity

For all measurements (n=92), the classification algorithm was capable of separating R$_{ROI}$, ER$_{ROI}$, and LR$_{ROI}$ (figure 3). Because LR$_{ROI}$ represented a larger proportion of pixels in the R$_{ROI}$ than ER$_{ROI}$, the R$_{ROI}$ temperature response more closely resembled the LR$_{ROI}$ temperature response (figure 8). The average time differences between the Time to T$_{max}$ computed for ER$_{ROI}$ and LR$_{ROI}$ of HV, ST, PC, and RC subject groups were 53 s, 73 s, 50 s, and 39 s, respectively (figure 8 b-c).

Calculated surrogate markers for the R$_{ROI}$, ER$_{ROI}$, and LR$_{ROI}$ are shown in tables 4, 5, and 6, respectively. Six key surrogate markers calculated for the R$_{ROI}$ were capable of separating the subject groups (figure 9).
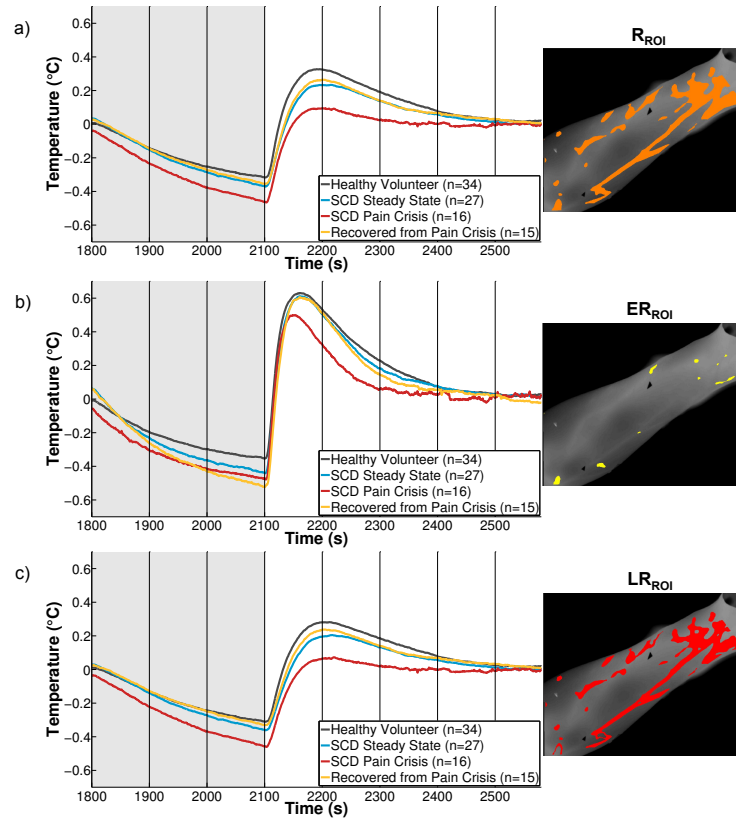
Fig. 8. *The group average temperature vs. time for (a) R_{ROI}, (b) ER_{ROI}, and (c) LR_{ROI} of HV, ST, PC, and RC subject groups. The occlusion time segment is highlighted in gray. Corresponding ROIs for a representative subject are shown on the right.*
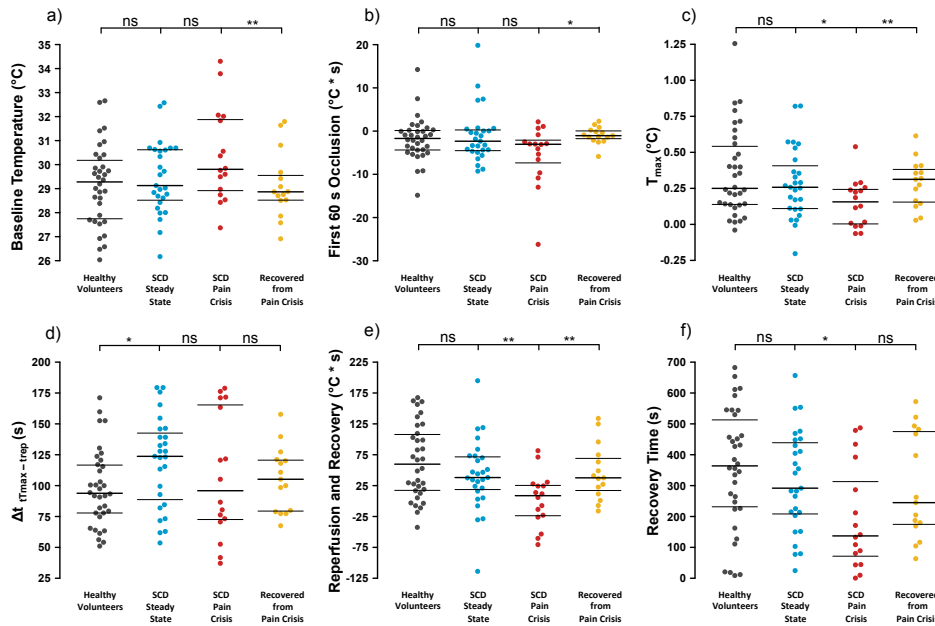
Fig. 9. *R_{ROI} surrogate markers capable of separating the subject groups: (a) Baseline Temperature, (b) First 60 s of Occlusion, (c) T_{max}, (d) $\Delta t_{tT'max-trep}$, (e) Reperfusion and Recovery, and (f) Recovery Time. Significance levels indicated by *p < 0.05, **p < 0.01, and ns (not significant).*

Table 4. Calculated R_{ROI} surrogate markers for HV, ST, PC, and RC groups. Data presented as median (interquartile range). p < 0.05 for ST compared to HV (*), PC compared to ST (†), and RC compared to PC (‡). Statistically significant comparisons between a subject group and the subject group immediately to its left are highlighted.

R_{ROI} Surrogate Marker	Healthy Volunteer (n=34)	Sickle Cell Steady State (n=27)	Sickle Cell Pain Crisis (n=16)	Recovered from Pain Crisis (n=15)
Baseline Temperature (°C)	29.3 (27.7, 30.3)	29.1 (28.5, 30.6)	29.8 (28.9, 31.9)	28.9 (28.5, 29.6)‡
First 60 s Occlusion (°C * s)	-1702 (-4390, 196)	-2339 (-4597, 372)	-3049 (-8121, -1679)	-1059 (-1924, 130)‡
T_{max} (°C)	0.25 (0.137, 0.56)	0.258 (0.108, 0.427)	0.156 (-0.001, 0.247)†	0.313 (0.15, 0.392)‡
$\Delta t_{tTmax-trep}$ (s)	94 (78, 117)	124 (87, 144)*	96 (72, 167)	105 (79, 121)
$\Delta t_{tT'max-trep}$ (s)	17 (15, 19)	19 (12, 29)	15 (12, 23)	19 (14, 31)
$\Delta t_{tTmax-tT'max}$ (s)	72 (57, 99)	105 (71, 121)*	69 (58, 129)	85 (64, 95)
Slope (m°C / s)	10.6 (8.3, 12.2)	8.5 (4.3, 9.8)*	7.7 (6.2, 11.2)	7.8 (5.2, 11.7)
Reperfusion and Recovery (°C * s)	59.7 (16.7, 109.5)	38.1 (17.4, 72.3)	8.7 (-24.5, 26.2)†	37.6 (14.3, 71.9)‡
First 30 s of Recovery	0.119 (0.061, 0.202)	0.104 (0.048, 0.178)	0.173 (0.094, 0.424)	0.139 (0.096, 0.188)
Recovery Time (s)	364 (226, 530)	292 (206, 443)	137 (62, 339)†	245 (172, 479)

Table 5. Calculated ER_{ROI} surrogate markers for HV, ST, PC, and RC groups. Data presented as median (interquartile range). p < 0.05 for ST compared to HV (*), PC compared to ST (†), and RC compared to PC (‡). Statistically significant comparisons between a subject group and the subject group immediately to its left are highlighted.

ER_{ROI} Surrogate Marker	Healthy Volunteer (n=34)	Sickle Cell Steady State (n=27)	Sickle Cell Pain Crisis (n=16)	Recovered from Pain Crisis (n=15)
Baseline Temperature (°C)	29.1 (27.9, 30.4)	29.5 (28.4, 30.8)	29.6 (29.4, 31.6)	29.3 (28.9, 30.7)‡
First 60 s Occlusion (°C * s)	-3053 (-6388, -449)	-2969 (-7774, 735)	-5651 (-10022, -3022)	-3534 (-6569, -975)
T_{max} (°C)	0.669 (0.409, 0.845)	0.606 (0.441, 0.962)	0.478 (0.37, 0.795)	0.647 (0.427, 0.893)
$\Delta t_{tTmax-trep}$ (s)	51 (37, 73)	61 (48, 76)	51 (38, 66)	72 (49, 87)
$\Delta t_{tT'max-trep}$ (s)	13 (12, 16)	11 (9, 21)	10 (9, 14)	18 (12, 20)
$\Delta t_{tTmax-tT'max}$ (s)	40 (24, 56)	50 (34, 65)	38 (28, 50)	54 (35, 64)
Slope (m°C / s)	22.1 (17, 32.2)	19.7 (16.5, 27)	22 (16.1, 28.4)	27.4 (14.9, 33.6)
Reperfusion and Recovery (°C * s)	86.6 (51, 147.4)	84.5 (66.2, 123.8)	61.4 (10.4, 79.1)†	53.4 (34.8, 161.4)
First 30 s of Recovery	0.169 (0.129, 0.217)	0.141 (0.081, 0.209)	0.283 (0.165, 0.391)†	0.189 (0.136, 0.262)
Recovery Time (s)	357 (258, 452)	329 (230, 488)	212 (108, 320)†	176 (141, 438)

Table 6. Calculated LR_{ROI} temporal markers HV, ST, PC, and RC groups. Data presented as median (interquartile range). p < 0.05 for ST compared to HV (*), PC compared to ST (†), and RC compared to PC (‡). Statistically significant comparisons between a subject group and the subject group immediately to its left are highlighted.

LR_{ROI} Surrogate Marker	Healthy Volunteer (n=34)	Sickle Cell Steady State (n=27)	Sickle Cell Pain Crisis (n=16)	Recovered from Pain Crisis (n=15)
Baseline Temperature (°C)	29.3 (27.7, 30.2)	29 (28.4, 30.5)	29.8 (28.8, 32)	28.8 (28.5, 29.5)‡
First 60 s Occlusion (°C * s)	-1549 (-3803, 666)	-1657 (-4015, 448)	-3023 (-8713, -1001)	-962 (-1566, -128)‡
T_{max} (°C)	0.233 (0.096, 0.491)	0.22 (0.101, 0.397)	0.12 (-0.006, 0.218)†	0.266 (0.14, 0.352)‡
$\Delta t_{tTmax-trep}$ (s)	104 (87, 137)	134 (89, 156)	101 (72, 154)	111 (94, 139)
$\Delta t_{tT'max-trep}$ (s)	18 (15, 23)	26 (18, 44)*	19 (12, 26)	23 (16, 36)
$\Delta t_{tTmax-tT'max}$ (s)	84 (67, 107)	104 (62, 120)	72 (60, 120)	72 (63, 115)
Slope (m°C / s)	7.6 (6, 9.7)	6.4 (4.2, 7.6)	6.5 (4.3, 8.5)	7 (4.5, 8.5)
Reperfusion and Recovery (°C * s)	55.2 (5.2, 96.1)	34.1 (9.7, 63.3)	4.1 (-31, 21.6)†	37.6 (11.9, 66.9)‡
First 30 s of Recovery	0.107 (0.071, 0.168)	0.081 (0.044, 0.137)	0.117 (-0.037, 0.213)	0.128 (0.08, 0.152)
Recovery Time (s)	365 (203, 518)	345 (198, 432)	131 (48, 341)†	267 (184, 480)

4. Discussion

In an attempt to delineate peripheral vascular dysfunction in sickle cell patients, we applied a PORH test combined with continuous IR imaging of the forearm (with subsequent image processing) to 92 subjects. Although LDF is a well-established technique for monitoring skin microvascular blood flow [12], its measurements of blood flow changes are reliable only in the small diameter vessels occurring within 0.3 mm of the surface. Additionally, LDF measurements may be confounded by skin pigmentation variability among subjects. Also, a slight shift in placement of LDF detector on the skin may cause substantial attenuation of the signal.

Compared to LDF flux, the prolonged temperature response to reperfusion may be the result of conduction of heat from deep (subcutaneous) vascular territories, including both small and large vessels. The observed general similarities between concurrently monitored LDF flux and IR temperature time profiles during the PORH occlusion, reperfusion, and recovery segments support the notion that skin temperature is a surrogate marker for blood flow changes (figure 6). Furthermore, photoplethysmographic measurement of relative blood volume in the middle finger after full forearm occlusion

on eleven HV subjects had a maximum response 120 s after reperfusion start [13], which is comparable to the $\Delta t_{tTmax - trep}$ of 94 s observed in the R_{ROI} of 34 HV subjects in our study.

The amplified reperfusion response observed in multiple areas on the skin surface during occlusion, reperfusion, and recovery (figure 5) allows speculation about functional architecture of reactive vasculature in the human forearm. Rapid decrease of the temperature in R_{ROI} may correspond to the collapse of these vessels during occlusion, and rapid increase of temperature in the same R_{ROI} may correspond to their recruitment during reperfusion and recovery. The location of ER_{ROI} on IR images may correspond to the projection of terminal arterioles, perforator vessels, and arteriovenous anastomoses on the skin surface. In fact, anastomoses and perforator angiosomes were recently thermographically identified as part of the human skin angioarchitecture [6]. The location of LR_{ROI} on IR images may correspond to veins connected to arteriovenous anastomoses, and other vessels with low resistance to blood flow during PORH test [14].

IR imaging allowed the quantification of reactive vasculature recruitment during reperfusion and recovery. As shown in figure 7, statistically significant differences were found between the PC (17.9% of pixels) and RC (13.4% of pixels) subject groups ($p < 0.01$) for skin areas with reactive vasculature. This can be interpreted as a higher recruitment of reactive vascular territories for the PC compared to the RC patients, which might reflect inflammatory state and a physiological vasomotor compensatory response to the elevated microvascular oxygen consumption during occlusion observed in the same PC group [15].

In an attempt to find differences in peripheral blood flow circulation between HV and SCD patients, 8 measurements were identified from IR-derived time-temperature profiles (table 1) which allowed us to calculate 50 surrogate markers related to peripheral temperature dynamics during the PORH test. Among these, only 13 surrogate markers statistically differed between HV vs. ST, ST vs. PC, and PC vs. RC subject groups (tables 3-6). The peak temperature response of the R_{ROI} during reperfusion ($\Delta t_{tTmax - trep}$) of the ST group was delayed by 30 s compared to the HV group (figure 9b, $p < 0.05$). This delay is comparable to a previous finding that peak LDF blood flow was delayed in ST subjects by an average of 23 s compared to HV subjects [10]. The lower maximum temperature during reperfusion (T_{max}) in PC group (figure 9a) compared to ST group ($p < 0.05$) and RC group ($p < 0.01$) was observed and can be interpreted as diminished peripheral blood flow capacity during pain crisis, which may be attributed to the presumed increased in blood viscosity during pain crises compared to steady state [16]. By looking at the differences in surrogate markers within the ER_{ROI} and LR_{ROI} (tables 5-6), we can attribute the differences seen within the R_{ROI} to specific types of vasculature, their remodeling, and the potential pathway of their autoregulation.

Due to the close relationship among skin temperature and changes in blood flow and the sensitivity of calculated surrogate markers to the condition of pain crisis in SCD, IR imaging may serve as a navigational tool for placement of point measurement detectors on areas of the human skin that are most sensitive to vascular perturbation. The observed temporal and spatial heterogeneity of the skin justifies placement of single point detectors [17] over the most reactive vessels, as isolating reactive regions revealed amplified hemodynamic signals and their differences between healthy and diseased states in this study. Potentially, this concept of targeted placement of wearable, wireless detectors can be utilized to identify and monitor prognostic indicators of peripheral vascular function in other diseases.

A major strength of our study is that it provides a passive, non-invasive imaging method capable of assessing spatial and temporal heterogeneity of skin blood flow in real time. Secondly, our study was conducted in 34 HV subjects, which may serve as a reference in studying blood flow in patients with other diseases. Third, we revealed vascular reactive sites in the skin where rapid and delayed temperature dynamics statistically differed between pairs of subject groups. And fourth, observed temporal and spatial diversity of blood-flow-derived forearm temperature allows proposing a new concept to use infrared imaging for targeted, individually-guided placement of skin sensors for much more sensitive monitoring of skin hemodynamics.

Our study has several limitations as well. The proposed segmentation of forearm vasculature was based on a functional, hemodynamic study. Further studies are required to improve understanding of the anatomical differences between reactive and non-reactive vasculature. Additionally, IR was used in this study solely as a surrogate measure of blood flow, although there may be other physiological factors that influence temperature dynamics of the forearm, such as local inflammation or thermogenic activity of dispersed brown fat. Further studies should look into the effects of these factors.

5. Conclusions

Application of the *k-means* algorithm to the original IR images revealed functional angioarchitecture of subcutaneous vasculature after reperfusion of the human forearm. Specifically, rapid and delayed responses in vascular clusters were identified. Statistically significant differences in IR-derived temperature surrogate markers in pairwise comparisons of HV, ST, PC, and RC subject groups were identified. Variation in occlusion, reperfusion, and recovery for different vascular beds of the forearm might explain the observed temporal and spatial diversity of post-occlusive responses in all subject groups. These findings may provide a platform for targeted investigation of vascular impairment in other diseases.

6. Acknowledgements

REFERENCES

[1] Tawfic Q. A., Faris A. S., Kausalya R., "The Role of a Low-Dose Ketamine-Midazolam Regimen in the Management of Severe Painful Crisis in Patients With Sickle Cell Disease". J Pain Symptom Manage, vol. 47, pp. 334-340, 2014.

[2] Hebbel R. P., Yamada O., Moldow C. F., Jacob H. S., White J. G., Eaton J. W., "Abnormal adherence of sickle erythrocytes to cultured vascular endothelium: possible mechanism for microvascular occlusion in sickle cell disease". J Clin Invest, vol. 65, pp. 154-160, 1980.

[3] Belhassen L., Pelle G., Sediame S., Bachir D., Carville C., Bucherer C., Lacombe C., Galacteros F., Adnot S., "Endothelial dysfunction in patients with sickle cell disease is related to selective impairment of shear stress–mediated vasodilation". Blood, vol. 97, pp. 1584-1589, 2001.

[4] Reiter C. D., Wang X., Tanus-Santos J. E., Hogg N., Cannon R. O. 3rd, Schechter A. N., Gladwin M. T., "Cell-free hemoglobin limits nitric oxide bioavailability in sickle-cell disease". Nat Med, vol. 8, pp. 1383-1389, 2002.

[5] Steinberg, M. H., "Management of Sickle Cell Disease". N Engl J Med, vol. 340, pp 1021-1030, 1999.

[6] Chubb D. P., Taylor G. I., Ashton M. W., "True and 'choke' anastomoses between perforator angiosomes: part II. dynamic thermographic identification". Plast Reconstr Surg, vol. 132, pp. 1457-1464, 2013.

[7] Gorbach A. M., Wang H., Elster E., "Thermal oscillations in rat kidneys: an infrared imaging study". Philos Transact A Math Phys Eng Sci, vol. 366, pp. 3633-3647, 2008.

[8] Gorbach A. M., Heiss J., Kufta C., Sato S., Fedio P., Kammerer W. A., Solomon J., Oldfield E. H., "Intraoperative infrared functional imaging of human brain". Ann Neurol, vol. 54, pp. 297-309, 2003.

[9] Gorbach A. M., Ackerman H., Liu W., Meyer J., Littel P., Seamon C., Footman E., Chi A., Zorca S., Krajewski M., Cuttica M., Machado R., Cannon 3rd R., and Kato G., "Infrared imaging of nitric oxide-mediated blood flow in human sickle cell disease". Microvasc Res, vol. 84, pp. 262-269, 2012.

[10] Rodgers G. P., Schechter A. N., Noguchi C. T., Klein H. G., Nienhuis A. W., Bonner R. F., "Microcirculatory adaptations in sickle cell anemia: reactive hyperemia response". Am J Physiol., vol. 258, pp. H113-H120, 1990.

[11] MacQueen, J., Some methods for classification and analysis of multivariate observations. Berkeley Symp on Math. Statist and Prob, vol. 1, pp. 281-297, 1967.

[12] Kuliga K. Z., McDonald E. F., Gush R., Michel C. C., Chipperfield A. J., Clough G. F., "Dynamics of microvascular blood flow and oxygenation measured simultaneously in human skin". Microcirculation, 2014.

[13] Selvaraj N., Jaryal A.K., Santhosh J., Anand S., Deepak K.K., "Monitoring of reactive hyperemia using photoplethysmographic pulse amplitude and transit time". J Clin Monit Comput., vol. 2009, pp. 315-322, 2009.

[14] Archaryya S., Archaryya K., "Spontaneous abdominal arteriovenous fistula and polysplenia in a child presenting with brain abscess". BMJ Case Reports, pp. 1-5, 2013.

[15] Rowley C. A., Ikeda A. K., Seidel M., Anaebere T. C., Antalek M. D., Seamon C., Conrey A. K., Mendelsohn L., Nichols J., Gorbach A. M., Kato G. J., Ackerman H., "Microvascular oxygen consumption during sickle cell pain crisis". Blood, 2014.

[16] Johnson, C.S., "Arterial Blood Pressure and Hyperviscosity in Sickle Cell Disease". Hematol Oncol Clin North Am., vol. 19, pp. 827-37, 2005.

[17] Webb R. C., Bonifas A. P., Behnaz A., Zhang Y., Yu K. J., Cheng H., Shi M., Bian Z., Liu Z., Kim Y. S., Yeo W. H., Park J. S., Song J., Li Y., Huang Y., Gorbach A. M., and Rogers J. A. Ultrathin conformal devices for precise and continuous thermal characterization of human skin. Nat Mater, vol. 12, pp. 938-944.